Provisioning in Multi-Band Optical Networks

Nicola Sambo, Alessio Ferrari, Antonio Napoli, Nelson Costa, João Pedro, Bernd Sommerkorn-Krombholz, Piero Castoldi, and Vittorio Curri

(Highly-Scored Paper)

***Abstract*—Multi-band (MB) optical transmission promises to extend the lifetime of existing optical fibre infrastructures, which usually transmit within the C-band only, with C+L-band being also used in a few high-capacity links. In this work, we propose a physical-layer-aware provisioning scheme tailored for MB systems. This solution utilizes the physical layer information to estimate, by means of the generalized Gaussian noise (GGN) model, the generalized signal-to-noise ratio (GSNR). The GSNR is evaluated assuming transmission up to the entire low-loss spectrum of optical fiber, i.e., from 1260 to 1625 nm. We show that MB transmission may lead to a considerable reduction of the blocking probability, despite the increased transmission penalties resulting from using additional optical fiber transmission bands. Transponders supporting several modulation formats (polarization multiplexing – PM – quadrature phase shift keying – PM-QPSK –, PM 8 quadrature amplitude modulation – PM-8QAM –, and PM-16QAM) from O- to L-band are considered. An increase of the accommodated traffic with respect to the C-band transmission only case, ranging from about four times with S+C+L-band and up to more than six times when transmitting from E to L-band is reported.**

***Index Terms*—Provisioning, blocking probability, multi-band, generalized Gaussian noise model.**

I. Introduction

SINGLE mode fibers (SMFs) present the minimum attenuation within the C-band, which has been one of the key-enablers for the success of optical communications. As the IP traffic continues increasing worldwide [2], solutions to cope with the enormous bandwidth demand are needed. One approach is to exploit the remaining low-loss windows – i.e., transmission bands beyond C – where SMF can propagate light in single mode.[1] First upgrades to L-band have been carried out for example in [4]. At the moment, advanced research is considering S- [5], [6] and U-band [7] for transmission. Recent improvements on optical components have demonstrated, for example, wideband amplifiers [8], [9] and transceivers [10] with improved optical performance. Moreover, MB transmission is also supported by the large amount of deployed optical fibers with negligible absorption peak at short wavelengths [11].

Until now, networking studies — e.g., on lightpath provisioning and routing and spectrum assignment — have focused mainly on C-band systems [12]–[16]. In particular, such studies aimed at selecting the proper route, portion of spectrum, and transmission parameters (including modulation format and code) in order to reduce the blocking probability in case of dynamic provisioning or, in general, to optimize spectrum occupancy in case of network design, while guaranteeing the proper quality of transmission and information rate. In such studies, the adopted physical layer models accounted for linear and nonlinear impairments. More specifically, regarding nonlinear impairments, self-phase modulation and cross-phase modulation have been mainly taken into account, as they are the dominant effects as shown in [17]. Then, several works dealt with routing and spectrum assignment assuming the Gaussian Noise model; examples of such works are [18]–[21]. However, when considering the neighbour bands, additional fiber transmission effects become relevant and, consequently, the physical layer modeling must be modified to take them also into account. For example, wideband nonlinear effects, such as stimulated Raman scattering (SRS) is not considered by the widely used Gaussian noise model. The generalized GN (GGN) [22], [23] can be used in this case, as it conservatively evaluates the amount of nonlinear interference when Raman scattering is not negligible. An accurate provisioning in MB networks can leverage enhanced physical layer models, such as GGN, and explore the different transmission performances within each transmission band for routing and spectrum assignment. Recently, authors in [24] and [25] investigated multi-band scenario with a specific reference to C+L systems, accounting for stimulated Raman scattering and amplified spontaneous emission noise generated by in-line amplifiers. Moreover, margin reduction in C+L systems and its benefits on the capacity is analyzed in [24] and [25]. More specifically, in [24], investigations on link margin

Manuscript received November 14, 2019; revised February 5, 2020 and March 17, 2020; accepted March 21, 2020. Date of publication March 30, 2020; date of current version May 6, 2020. This work was supported in part by the H2020 Metro-Haul Project 761727 and in part by the European Union Horizon 2020 research and innovation program under the Marie Skłodowska-Curie ETN WON, Grant Agreement 814276. This paper is an extended version of [1]. *(Corresponding author: Nicola Sambo.)*

Nicola Sambo and Piero Castoldi are with the Scuola Superiore Sant'Anna, 56124 Pisa, Italy (e-mail: nicola.sambo@sssup.it; castoldi@sssup.it).

Alessio Ferrari and Vittorio Curri are with the Politecnico di Torino, 10129 Torino, Italy (e-mail: alessio.ferrari@polito.it; vittorio.curri@polito.it).

Antonio Napoli and Bernd Sommerkorn-Krombholz are with Infinera, 81541 Munich, Germany (e-mail: anapoli@infinera.com; BSommerkorn@infinera.com).

Nelson Costa is with Infinera Unipessoal Lda., 2790-078 Carnaxide, Portugal (e-mail: NCosta@infinera.com).

João Pedro is with Infinera Unipessoal Lda., 2790-078 Carnaxide, Portugal, and also with Instituto de Telecomunicações, Instituto Superior Técnico, 1049-001 Lisboa, Portugal (e-mail: jpedro@infinera.com).

Color versions of one or more of the figures in this article are available online at http://ieeexplore.ieee.org.

Digital Object Identifier 10.1109/JLT.2020.2983227

[1]The single-mode spectrum of SMF starts at 1260 nm [3]. We define a system capable of transmitting from O → L-band as multi-band (MB).

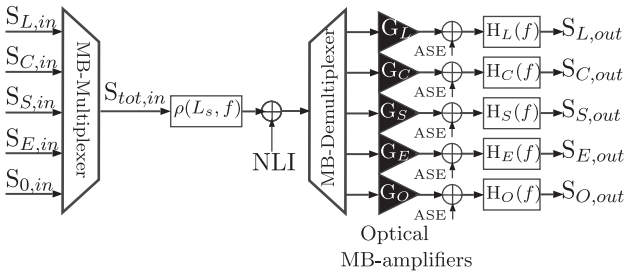

Fig. 1. Equivalent block diagram of the considered span for a MB- optical system.

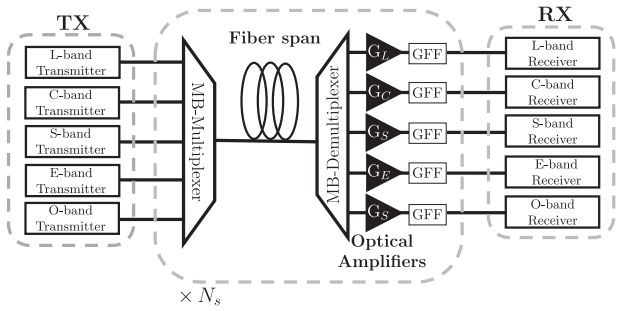

Fig. 2. Considered block diagram used to estimate the propagation impairments.

reduction are included. In [25], the selection of channel launch power accounting for the actual spectrum occupation is analyzed instead of the commonly adopted assumption of all channels lit on. Multi-band optical networks are attracting the interest of network operators as a alternative way of increasing fiber life and studies are still needed on other bands such as S, E, and O, and on the strategies for lightpath allocation.

The goal of this manuscript is to explore MB transmission leveraging the existing optical fiber infrastructure for capacity increase of optical networks. In [1], we proposed a provisioning strategy for MB optical networks exploiting the low-loss regions of optical fiber beyond the C-band (e.g., from S $\rightarrow$ L-band). In this contribution, we extend our previous work (i) by adding the additional O- and E-band; (ii) by introducing a study which includes a further modulation format besides PM-QPSK and PM-16QAM, i.e. PM-8QAM; (iii) by providing a more detailed analysis of the blocking probability and the spectrum utilization. With this aim, we carried out a comprehensive numerical analysis to assess the reduction of the blocking probability enabled by MB transmission. Our results show that MB-based systems can accommodate more traffic despite the degradation of the generalized optical signal-to-noise-ratio (GSNR), in C-band, caused by the use of more bands. In the framework of this paper, we consider the following four MB upgrade scenarios: (C+L), (C+L+S), (C+L+S+E), (C+L+S+E+O)-band. The GSNR is estimated through the GGN model as described by Eq. 4 of [22].

By exploiting the GSNR as a metric, we evaluate the MB-based provisioning strategies when transmitting from O $\rightarrow$ L-band. A detailed analysis based on PM-QPSK, PM-8QAM, and PM-16QAM over the aforementioned scenarios is provided, demonstrating an increase of accommodated traffic from four to more than six times with respect to C-band only.

The remainder of the paper is organized as follows: Section II describes the physical layer model and the considered MB system. Section III presents the adopted provisioning strategy for MB optical networks and Section IV reports the numerical results for different upgrade scenarios in terms of band occupancy and modulation format. Section V draws the conclusions.

II. Physical Layer Modeling and Considered Network

We abstract each span of the considered network as depicted in Fig. 1. The signals in each band are multiplexed by a MB-Mux and the resulting signal, $\mathrm{S}_{tot,in}$, is launched into the optical fiber. The optical fiber is modeled by the transfer function, $\rho(L_s, f)$, and by a source of noise (resulting from nonlinearities – NLI). $\rho(L_s, f)$ includes both the fiber attenuation and the SRS and it is evaluated numerically solving the ensemble of ordinary differential equations describing the SRS [26], while the noise source models the Kerr effect, which is evaluated according to the GGN model [27]. After optical fiber propagation, each band is de-multiplexed by a MB-demux and amplified by the per-band-optimized doped-fiber-amplifier (DFA). Every amplifier is abstracted with a flat gain G, an additive amplified spontaneous emission (ASE) noise source and a transfer function modelling the gain flattening filter (GFF). In this case, the GSNR of a single fiber span (GSNR_s) can be computed as

$$\mathrm{GSNR}_s = \frac{P_{in} \times \rho(L_s, f)^2 \times \mathrm{G} \times H(f)}{P_{\mathrm{ASE}} \times H(f) + P_{\mathrm{NLI}} \times \mathrm{G} \times H(f)}, \quad (1)$$

where P_{in} is the signal power at the input of the fiber, P_{ASE} is the ASE noise power, P_{NLI} is the NLI power and $H(f)$ is the GFF transfer function. The physical impairment introduced by each re-configurable optical add-drop multiplexer (ROADM) node is modelled as an attenuation introduced by the passive components of the node and a booster amplifier which recovers the node loss and introduces additional ASE noise. Thus, we define a GSNR of the ROADM node, GSNR_n, as

$$\mathrm{GSNR}_n = \frac{P_{in} \times L_{\mathrm{ROADM}} \times G_{\mathrm{BST}}}{P_{\mathrm{ASE}}}, \quad (2)$$

where P_{in} is the signal power at the input of the ROADM node, L_{ROADM} is the node loss, G_{BST} is the booster gain and P_{ASE} the ASE noise introduced by the booster amplifier. To compute the GSNR of a lightpath (LP), we assume the incoherent accumulation of noise. Thus, the GSNR of a LP is computed as [28]

$$\begin{aligned} \mathrm{GSNR} &= \left(\sum_{s \in \mathrm{path}} \mathrm{iGSNR}_s + \sum_{n \in \mathrm{path}} \mathrm{iGSNR}_n \right)^{-1} \\ &= \left(\sum_{s \in \mathrm{path}} (\mathrm{GSNR}_s)^{-1} + \sum_{n \in \mathrm{path}} (\mathrm{GSNR}_n)^{-1} \right)^{-1}, \end{aligned} \quad (3)$$

where iGSNR is the inverse of GSNR, the index s indicates the s-th span belonging to the path of the LP and the index n indicates the n-th node.

TABLE I
MAIN MB SYSTEM PARAMETERS

Band	O	E	S	C	L
Wavelength range [nm]	1260 - 1360	1360 - 1460	1460 - 1530	1530 - 1565	1565 - 1625
Frequency range [THz]	220.59 - 238.10	205.48 - 220.59	196.08 - 205.48	191.69 - 196.08	184.62 - 191.69
Used bandwidth [THz]	12	14.8	9.1	4.05	6.95
Central frequency [THz]	229.35	213.04	200.78	193.89	188.16
Slices @ 12.5 GHz	960	1184	732	332	548
Noise figure [dB]	7	6	7	5.5	6
Type of amplifier	PDFA [30]	BDFA [31]	TDFA [29]	EDFA	EDFA
Nonlinear coefficient γ [1/W/km]	1.6	1.5	1.4	1.3	1.28

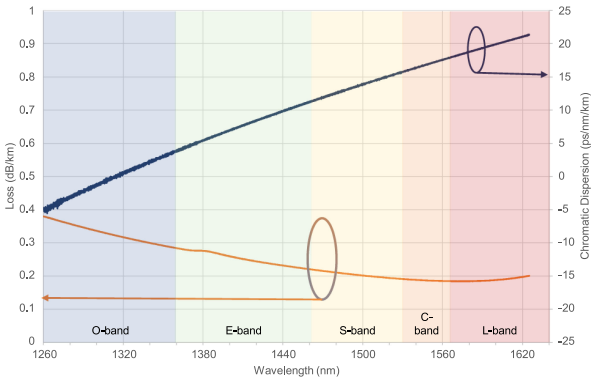

Fig. 3. Attenuation and dispersion versus lambda from O- to L-band for a ITU G.652D fiber.

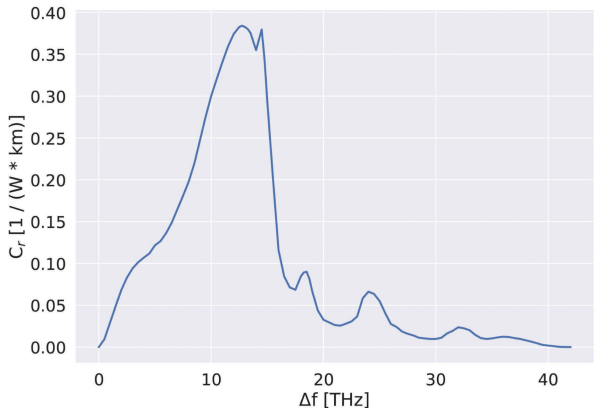

Fig. 4. Raman coefficient vs. Δf.

Fig. 2 depicts the high level setup for a MB optical system, used to estimate the propagation impairments in the network. The setup is composed of a MB transmission bench consisting of {O, E, S, C, L}-band transmitters. A flexible grid with 12.5 GHz of bandwidth granularity is assumed. A net data-rate of 200 Gb/s is considered enabled by PM-16QAM at 32 Gbaud symbol rate (one carrier in 37.5 GHz), PM-8QAM at 43 Gbaud (one carrier in 50 GHz), and PM-QPSK at 32Gbaud (two carriers in 75 GHz). The selected roll-off factor is 0.15. A 1.85 nm guard-band between all adjacent bands is considered. At the receiver side, the bands are de-multiplexed, amplified, optically equalized (via a GFF) and finally demodulated. The ITU wavelength ranges, number of 12.5 GHz slices, and noise figures (NF) of the considered optical amplifiers are reported in Table I. We assume lumped amplification only with Erbium doped fiber amplifiers (EDFA) in C- and L-bands; Thulium DFA (TDFA) in S-band [29]; Praseodymium DFA (PDFA) in E-band [30]; and finally Bismuth DFA in O-band [31]. It has been assumed that the fiber is SMF type having an effective core area of 80 μm^2, the attenuation coefficient and the dispersion are depicted in Fig. 3, the non-linear coefficient is reported in Table I and the Raman coefficient is shown in Fig. 4.

Regarding optical nodes, the widely adopted *broadcast and select* or *switch and select* architectures can be assumed [32]. In such nodes, switching (and also add and drop) is performed based on wavelength selective switches (WSSs). Commercial WSSs are already available operating in C+L-band. The development of WSSs operating in S-, E-, and O-bands depends on the opportunities that such bands offer to increase the fiber life-time and capacity. This work will also provide some insight to this open issue.

III. PROVISIONING IN MULTI-BAND OPTICAL NETWORKS

A flex-grid optical network is assumed with transponders supporting multiple modulation formats, symbol rates, and codes. O-, E-, S-, C-, and L-bands can be exploited for lightpath provisioning implying specific levels of quality of transmission (QoT) depending on the used bands. We abstract the QoT over each lightpath using the GSNR as it is the well-accepted unique figure of merit for the QoT [33], so the overall GSNR on a lightpath is given by the GSNR degradation of each crossed line transmission system [34].

The proposed provisioning scheme for MB optical networks is summarized by the flow chart in Fig. 5. Upon a connection request from source *s* to destination *d*, a path is computed (e.g., shortest path). Then, the modulation format with the highest spectral efficiency (e.g., PM-16QAM) is selected. Next, the spectral region (i.e., the transmission band) is chosen, where preference to a specific band can be assigned. For instance, we could start by filling in first the C-band, afterwards the L-band and so on, till all bands are filled. Afterwards, quality of transmission (QoT) is evaluated. In this work, we rely on the QoT-estimator (QoT-E) of GNPy [35], an open source software for assessing the physical layer of modern optical networks. Such a library evaluates the NLI by means of the GGN model – shown in [22] – as it is accurate and conservative when chromatic dispersion roughly exceeds 5 ps/nm/km [36]. For lower dispersion values – the O-band, in our analysis – the GGN model inaccuracy can be larger because of the large correlation between the NLI generated by subsequent fiber spans. But in case of operating the O-band together with the adjacent bands, all at lower frequencies, the O-band channels are fast depleted by

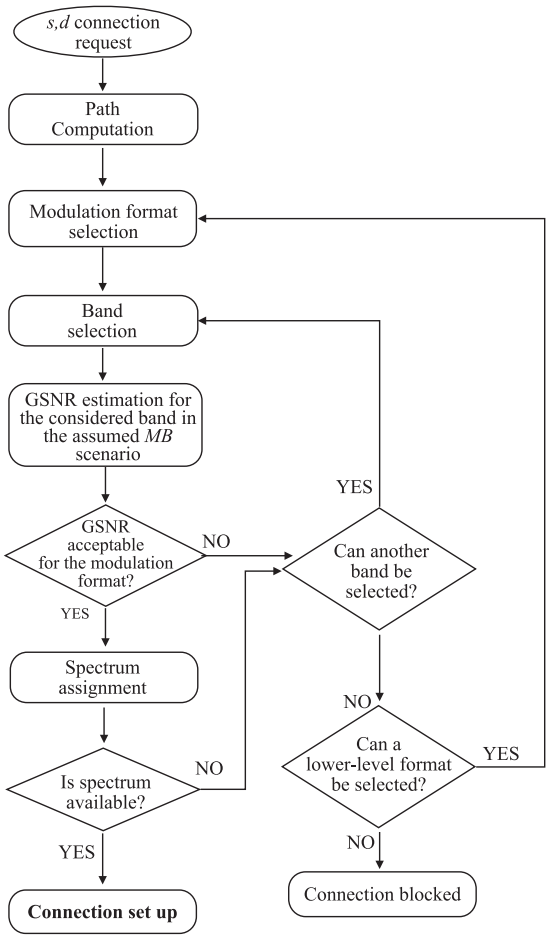

Fig. 5. Flow chart of the proposed provisioning scheme.

first- and higher-order SRS-induced power transfer. So O-band channels' performance is always dominated by the ASE noise keeping the NLI practically irrelevant. As a consequence, an underestimation of the NLI will have a negligible impact on the GSNR. Other NLI models could be adopted, e.g., [37], [38], [39], provided that the interaction between SRS-induced power transfer and NLI generation are properly addressed. The GSNR is estimated numerically for the selected scenario using the GGN model. Its value depends on: (i) the computed path; (ii) the MB scenario (e.g., C+L+S); and (iii) the considered band, as will be shown in the next section. If the estimated GSNR is sufficient to guarantee error-free transmission for the considered modulation format (i.e., above a pre-defined threshold) in the selected band and for the considered MB transmission scenario, the spectrum assignment (SA) is executed (e.g., first fit) within the selected band. On the other hand, if GSNR is below the threshold or if no spectrum satisfying the continuity constraint is available in the considered band, another transmission band is selected and the GSNR is re-evaluated. If the estimated GSNR is below the threshold in all considered bands, a modulation format with lower GSNR requirements is selected (e.g., PM-8QAM), implying smaller spectral efficiency. If sufficient GSNR cannot be guaranteed for any of the available modulation formats or if the continuity constraint cannot be met in any of the transmission bands, the connection is blocked.

Regarding the complexity of the provisioning scheme, this mainly depends on the complexity of the GGN model and of the path computation algorithm, and on the number of frequency 12.5-GHz slices considered for spectrum assignment. The QoT has been computed by using the QoT-estimator of the GNPy library [35] whose complexity increases linearly with the number of channels. Regarding path computation, if we assume a shortest path algorithm such as Dijkstra [40] used in the simulations, the complexity is $O(\|E\| + \|V\| \log \|V\|)$ where E and V are the number of arches and nodes in the topology, respectively. Consider that the shortest paths can be pre-computed and their QoT pre-validated by the GGN model. Finally, the complexity of spectrum assignment is $O(SL)$ where S is the number of 12.5-GHz frequency slices and L the number of links in the path.

IV. Simulation Results

A custom built event-driven C++ simulator has been used to evaluate the blocking probability of C+L, C+L+S, C+L+S+E, and C+L+S+E+O MB transmission scenarios versus the widely used C-band only. Simulations have been carried out on a Intel(R) Core(TM) i5 @2.67 GHz, with 4 RAMs of 4 GB. We tested the proposed provisioning scheme on a reference Spanish transport network with 30 nodes and 55 bi-directional links [41], all composed of standard SMF (SSMF). Each span is 80 km long. The inter-arrival process of 200 Gb/s connection requests is assumed to be Poissonian. Inter-arrival and holding times are exponentially distributed with an average of $1/\kappa$ and $1/\mu = 500$ s, respectively, with the connection requests uniformly distributed among all node pairs. Traffic load is expressed as κ/μ. Shortest path is considered for path computation while first fit is adopted for SA, i.e., the lowest indexed available portion of spectrum satisfying the continuity constraint in the considered band, is selected.

The following modulation formats and symbol rates are considered: 1) only PM-QPSK at 32 Gbaud; 2) only PM-16QAM at 32 Gbaud; 3) PM-16QAM and PM-QPSK, both at 32 Gbaud; 4) PM-16QAM and PM-QPSK at 32 Gbaud and PM-8QAM at 43 Gbaud. The same FEC overhead of 21% is assumed in all cases. Single carrier transmission is adopted for PM-16QAM and PM-8QAM, while dual carrier is assumed for PM-QPSK, thus always guaranteeing a 200 Gb/s net rate. We assume 200 Gb/s connections using 37.5 GHz, 50 GHz, and 75 GHz if PM-16QAM, PM-8QAM, or PM-QPSK is adopted, respectively. For simplicity, we set a per-band power with flat spectral load [42]. Only the GSNR of the worst channel (also considering cross-phase modulation) is assumed for each band. This way, when new channels are set up, any existing lightpath will still show acceptable performance thus avoiding possible reconfigurations. Other strategies (e.g., based on the actual spectral occupation) could be instead adopted [25]. The power values are reported in Table II. Assuming the pre-FEC BER threshold 4×10^{-3}, according to the theoretical BER-vs-GSNR curve, the following threshold values are considered for the GSNR:

TABLE II
TRANSMITTED POWER PER CHANNEL PER BAND

Scenario / Band	L	C	S	E	O
C only	–	15.23	–	–	–
C+L	13.88	15.04	–	–	–
C+L+S	12.31	13.91	13.83	–	–
C+L+S+E	11.43	12.91	13.0	10.99	–
C+L+S+E+O	11.18	12.67	12.74	10.90	3.43

TABLE III
PER-BAND WORST-CASE GSNR [DB] FOR A SAMPLE 960-KM SSMF PATH, WITH SPAN LENGTH OF 80 KM, WHEN 32 GBAUD SYMBOL RATE IS ASSUMED

O	E	S	C	L
-0.9 dBm	-1.1 dBm	-1.0 dBm	-1.7 dBm	-1.0 dBm

15.1 dB for PM-16QAM, 12.5 dB for PM-8QAM, and 8.5 dB for PM-QPSK.

Table III reports the estimated GSNR for the worst-case channel per band in a 960 km-long SSMF route from the considered topology when 32 Gbaud symbol rate is adopted. Using the L-band in addition to the C-band depletes the C-band due to Raman scattering. However, only a small penalty is observed because the Raman effect impacts mostly the highest frequencies of C-band which are the best performing ones when C-band only transmission is adopted because of SRS as shown in [22]. On the other hand, using also the S-band triggers a considerable power transfer to C- and L-bands – still due to Raman effect, leading to higher NLI in C- and L-bands. When we switch on also the E- and O-bands, the SRS and the higher fiber attenuation in these bands decrease significantly the performance of these bands (with respect to the remaining ones) due to the high reduction of the available channel power. When a 43 Gbaud symbol rate is adopted instead of 32 Gbaud, similar GSNR values are obtained, thus they are not reported. As an example, for the same path in Table II, a GSNR of 13.6 dB is estimated in the C-band, instead of 13.91 dB, when the C+L+S-band transmission scenario is considered.

The following strategies are considered for the *band selection* step in Fig. 5. For each MB scenario and strategy, bands are provided from the most preferred to the less preferred. *C preferred – C+L*: consists in a C+L multi-band scenario where C is preferred to L; *L preferred – C+L*: L, C; *C preferred – C+L+S*: consists in a C+L+S scenario where C is preferred, then L, and finally S; *L preferred – C+L+S*: L, C, S; *C preferred – C+L+S+E*: consists in a C+L+S+E scenario where C is preferred, then L, S, and finally E; *C preferred – C+L+S+E+O*: C, L, S, E, O. The performance are collected through 100 experiments of 10000 connection requests; plots are reported with a confidence interval of 95%.

Fig. 6 shows the blocking probability versus traffic load when only PM-QPSK is supported and *C preferred* is considered (in C+L and C+L+S-band transmission scenarios). Clearly, the exploitation of MB transmission strongly reduces the blocking probability. Indeed, although the exploitation of L- and L+S-bands impacts the GSNR in C-band (as illustrated in Table II), the resulting penalty does not implies the infeasibility of any path in the C-band when only PM-QPSK is transmitted. Thus,

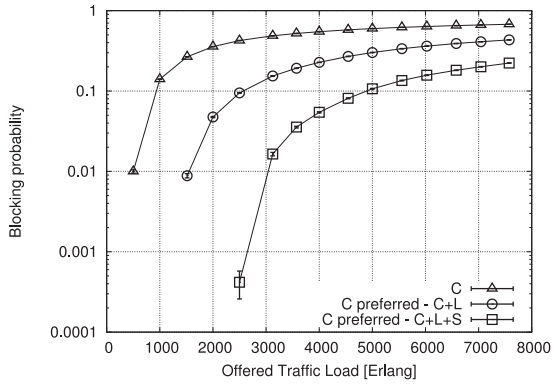

Fig. 6. Blocking probability versus traffic load when C is preferred and with PM-QPSK only.

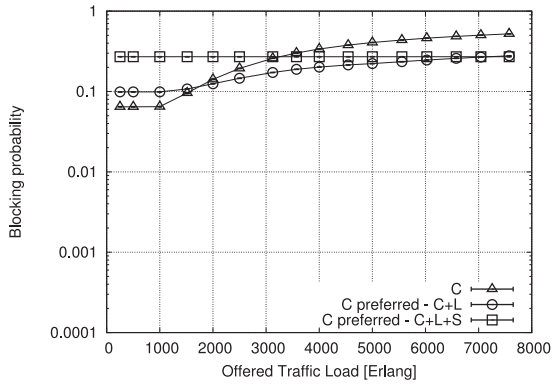

Fig. 7. Blocking probability versus traffic load when C is preferred and with PM-16QAM only.

the blocking probability decreases significantly in the C+L and even further in the C+L+S-band transmission scenarios. This is not the case when only PM-16QAM is used.

Fig. 7 shows the blocking probability when only PM-16QAM is supported and *C preferred* in C+L and C+L+S MB transmission scenarios are considered. In this case, Fig. 7 shows a blocking floor at small loads. This result is a consequence of having paths that are unfeasible with PM-16QAM (even when C-band only transmission is considered) due to the higher QoT requirements of PM-16QAM with respect to PM-QPSK (the GSNR threshold is ∼15 dB instead of ∼8 dB). Moreover, MB transmission leads to additional GSNR penalty in the C-band, which implies an even higher number of unfeasible paths, thus leading to an increase of the blocking floor in the MB transmission scenarios. This result indicates that the availability of different modulation formats can be key to efficiently exploit MB transmission.

Fig. 8 depicts the blocking probability versus traffic load when both PM-16QAM and PM-QPSK are supported. The *C preferred* and *L preferred* approaches are also compared. Focusing on *C preferred*, the support of multiple modulation formats permits to achieve lower blocking probability than the one reported in Figs. 6 and 7. Indeed, when PM-16QAM is feasible, only 37.5 GHz are occupied per connection instead of 75 GHz, thus

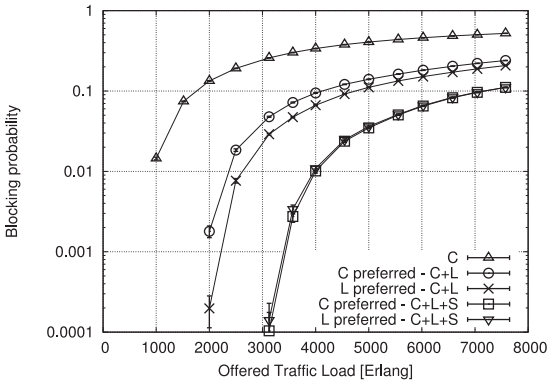

Fig. 8. Blocking probability versus traffic load with both PM-16QAM and PM-QPSK.

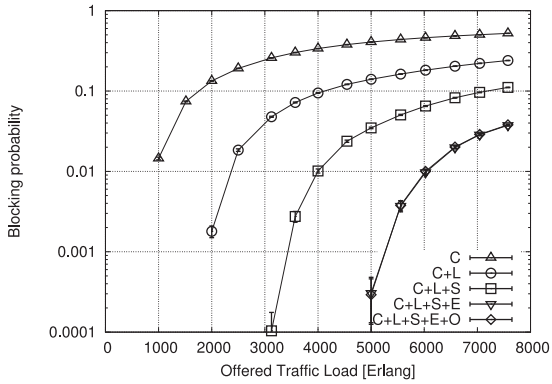

Fig. 9. Blocking probability versus traffic load with both PM-16QAM and PM-QPSK considering C, L, S, E, and O-bands.

improving spectral efficiency. As an example, the comparison of Figs. 6 and 8 shows that using PM-16QAM, besides PM-QPSK, results in a blocking probability of about 0.01 instead of almost 0.1 at 4000 Erlang in the C+L+S-band transmission scenario. Moreover, when the GSNR is smaller than 15.13 dB, the more relaxed PM-QPSK is exploited to avoid the blocking floor reported in Fig. 7.

Fig. 8 indicates also that it may be useful to prefer L- to C-band during provisioning when C+L-band transmission is considered. This result is a consequence of having paths that are feasible with PM-16QAM in C-band, but not in L-band, due to the worse optical performance in the latter band. With *C preferred*, C-band is rapidly filled and it may happen that a connection that would be feasible with PM-16QAM in C-band must adopt L-band instead and, consequently, PM-QPSK. On the contrary, *L preferred* results in a maximization of the number of connections using PM-16QAM due to the mode of operation of the proposed provisioning scheme summarized in Fig. 5. Fig. 8 illustrates also the potential of S-band to increase the capacity of a network. Indeed, about a fourfold increase of the provisioned traffic is reported when considering C+L+S-band transmission instead of C-band only, at a blocking probability of 10^{-2}. This increment is slightly less than the overall increment of spectrum when adding L and S bands. Indeed, looking at Table I, the number of 12.5-GHz slices increases by a factor of around 4.8 when activating L and S bands. Differently, the load increases by a factor of 4 because of the poorer physical performance of the L band and because the number of accepted lightpaths also depends on the traffic matrix and some spectrum could be left unused since continuity constraint is not satisfied along the links.

The exploitation of additional optical fiber bands for data transmission is analyzed in the following. Fig. 9 depicts the blocking probability versus traffic load when several MB transmission scenarios are considered, including also E- and O-bands transmission, with *C preferred*. Both PM-16QAM and PM-QPSK are used in this case. Fig. 9 shows that exploiting E-band strongly reduces blocking probability. On the contrary, the exploitation of O-band in the considered topology does not bring any benefit. Indeed, C+L+S+E and C+L+S+E+O-band transmission present the same blocking probability. This result

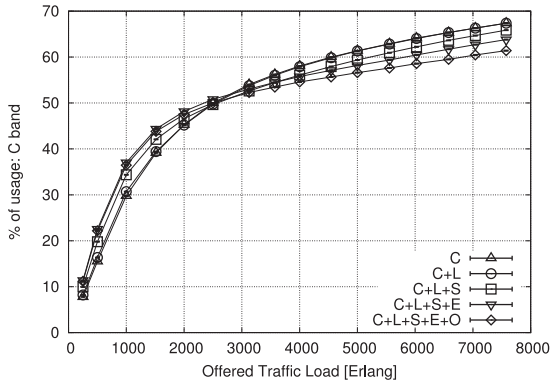

Fig. 10. Percentage of spectrum utilization in the C-band vs. traffic load.

is a consequence of the small GSNR available in O-band. As an example, Table II reports a GSNR of only 3.43 dB in the O-band versus 10.9 dB in the E-band. For the C+L+S+E and C+L+S+E+O scenarios, we investigated also *E preferred* (i.e., E preferred to C, then L, S, and finally O): this band selection strategy presents similar performance than *C preferred*, thus the related plot is not shown. Additional results are provided in the following to provide more insights on the usage of the several bands.

Figs. 10–13 show the percentage of spectrum utilization in the C, L, S, and E-bands, respectively, for all the considered MB transmission scenarios with *C preferred*, averaged on all network links. Regarding C-band utilization (Fig. 10), the activation of S- and E-bands implies an higher spectrum utilization at low loads because the GSNR in C-band becomes smaller and more paths require the selection of PM-QPSK, which requires more spectrum. At higher loads, and with the saturation of C-band, lightpaths need to use other bands. For this reason, and also due to the worse physical performance, C-band is slightly less utilized at higher loads when more bands are exploited.

Spectrum utilization in the L-band (Fig. 11) also increases as more bands are activated. Again, the activation of more bands implies a reduction of GSNR in the L-band. This is caused by the power transfer from the higher frequency channels to the lower frequency ones due to stimulated Raman scattering.

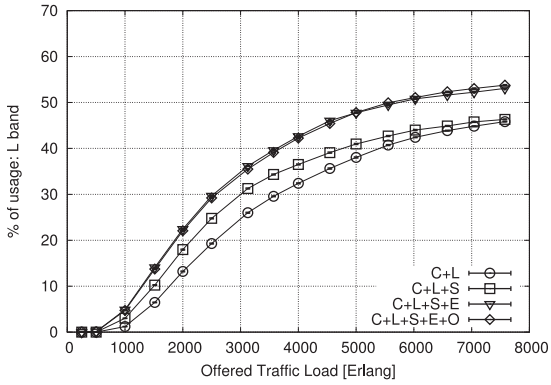

Fig. 11. Percentage of spectrum utilization in the L-band vs. traffic load.

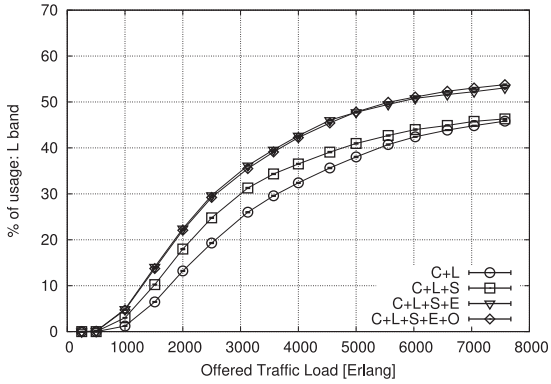

Fig. 12. Percentage of spectrum utilization in the S-band vs. traffic load.

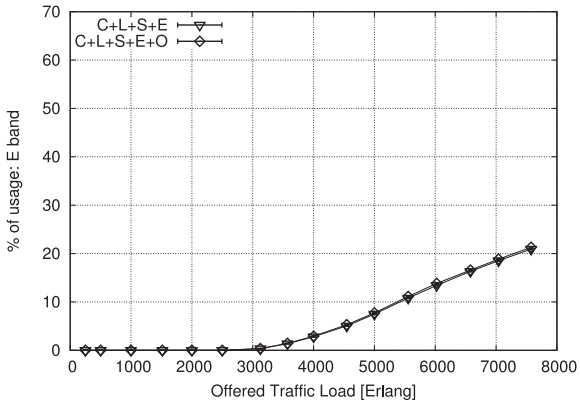

Fig. 13. Percentage of spectrum utilization in the E-band vs. traffic load.

This increases the power of the L-band channels while the population of other bands grows. This causes higher NLI generation in the L-band, which leads to a lower GSNR. Thus, more lightpaths have to rely on PM-QPSK modulation consequently occupying more spectrum. The same behavior occurs in the S-band (Fig. 12). The utilization of E-band (Fig. 13) does not change with the activation of O-band because the last one is actually never used, due to the degraded optical performance. By comparing the overall utilization of C, L, S, and E-bands, we find that it follows the ranking of preference for band selection: C, L, S, and, finally, E-band.

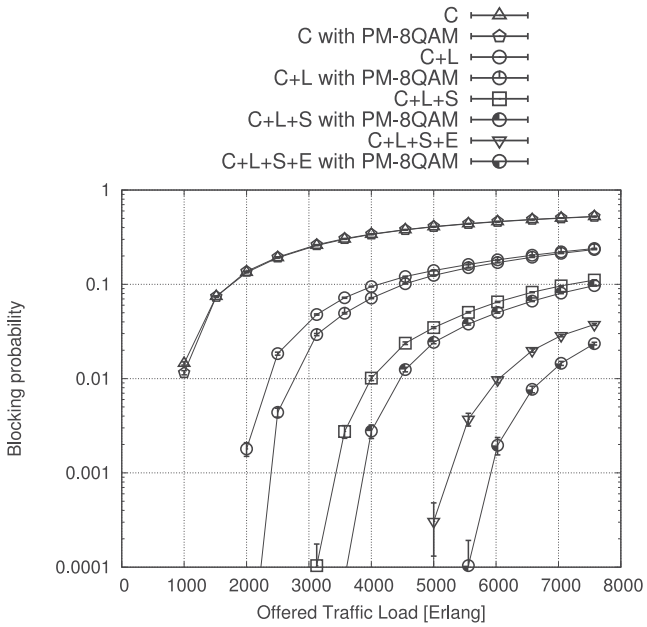

Fig. 14. Blocking probability versus traffic load when PM-8QAM is available and with *C preferred*.

Finally, the exploitation of an additional modulation format (PM-8QAM) is also investigated. Fig. 14 depicts the blocking probability versus traffic load when PM-8QAM modulation format is also considered. In particular, when PM-8QAM is referred to in Fig. 14, all three modulation formats are available, otherwise only PM-16QAM and PM-QPSK can be selected. Fig. 14 shows that the exploitation of this additional modulation format, with different robustness to transmission impairments and spectrum efficiency, offers more possibilities for adaptation to the GSNR experienced along a route and in a specific multiband scenario, thus improving the blocking probability with respect to the case of selecting only PM-QPSK and PM-16QAM. For the selected topology, relevant benefits are reported especially in the C+L+S+E-band transmission scenario, which is the more performance demanding. In the case of C band only, the routing and spectrum assignment is accomplished in less than one millisecond, while in the order of few milliseconds in the C+L+S+E case.

V. Conclusions

We have presented a provisioning scheme for multi-band optical networks leveraging the GGN model and taking into account the stimulated Raman scattering. Simulation results have shown that up to four times more traffic can be carried in a network when using C-, L- and S-bands for data transmission. An additional increase of accommodated traffic is experienced through the use of E-band. On the other hand, O-band does not offer sufficient signal quality for transmission distances comparable to the ones of regional and backbone networks. Therefore, the reported results suggest that, in the medium term, an enhancement of

the enabling technologies for S-band (e.g., WSSs) may extend the lifetime of existing optical fibre infrastructures. Moreover, efforts on the development of devices operating in the E-band may further enable significant network capacity increase. On the contrary, the development of enabling technologies for O-band does not seem justified (for transmission distances comparable to the ones of regional and backbone networks). Lastly, an increased granularity in the available modulation formats is desirable as it enables further reducing the blocking probability in MB transmission scenarios.

REFERENCES

[1] N. Sambo *et al.*, "Provisioning in multi-band optical networks: A C+L+S-band use case," in *Proc. Eur. Conf. Opt. Commun.*, 2019, pp. 1–4.

[2] "Cisco Visual Networking Index: Forecast and Methodology," Jun. 2017. [Online]. Available: https://www.cisco.com/c/en/us/solutions/service-provider/visual-networking-index-vni/index.html

[3] "Handbook – Optical fibres, cables and systems - ITU," 2009. [Online]. Available: https://www.itu.int/dms_pub/itu-t/opb/hdb/T-HDB-OUT.10-2009-1-PDF-E.pdf

[4] "Windstream Deploys Infinera C+L Solution, Sets Foundation to Double Fiber Capacity," Oct. 2018. [Online]. Available: https://www.infinera.com/press-release/windstream-deploys-infinera-c-l-solution-sets-foundation-double-fiber-capacity

[5] J. Renaudier and A. Ghazisaeidi, "Scaling capacity growth of fiber-optic transmission systems using 100+ nm ultra-wideband semiconductor optical amplifiers," *J. Lightw. Technol.*, vol. 37, no. 8, pp. 1831–1838, 2019.

[6] F. Hamaoka *et al.*, "Ultra-wideband WDM transmission in S-, C-, and L-bands using signal power optimization scheme," *J. Lightw. Technol.*, vol. 37, no. 8, pp. 1764–1771, 2019.

[7] A. Ferrari *et al.*, "Upgrade capacity scenarios enabled by multi-band optical systems," in *Proc. 21st Int. Conf. Transparent Opt. Netw.*, 2019, pp. 1–4.

[8] E. M. Dianov, "Amplification in extended transmission bands using bismuth-doped optical fibers," *J. Lightw. Technol.*, vol. 31, no. 4, pp. 681–688, 2012.

[9] D. F. Bendimerad *et al.*, "Feasibility study of wide-band in-line SOA amplification for PDM-MQAM long-haul WDM transmission systems," in *Proc. 39th Eur. Conf. Exhib. Opt. Commun.*, 2013, pp. 1–3.

[10] C. Doerr *et al.*, "O, E, S, C, and L band silicon photonics coherent modulator/receiver," in *Proc. Optical Fiber Commun. Conf. Exhib.*, 2016, pp. 1–3.

[11] "Increasing data traffic requires full spectral window usage in optical single-mode fiber cables," TE Connectivity Broadband Network Solutions – EMEA, White paper, 2014.

[12] B. C. Chatterjee, N. Sarma, and E. Oki, "Routing and spectrum allocation in elastic optical networks: A tutorial," *IEEE Commun. Surv. Tut.*, vol. 17, no. 3, pp. 1776–1800, Jul.–Sep. 2015.

[13] K. Christodoulopoulos, I. Tomkos, and E. A. Varvarigos, "Elastic bandwidth allocation in flexible OFDM-based optical networks," *J. Lightw. Technol.*, vol. 29, no. 9, pp. 1354–1366, May 2011.

[14] M. Klinkowski and K. Walkowiak, "Routing and spectrum assignment in spectrum sliced elastic optical path network," *IEEE Commun. Lett.*, vol. 15, no. 8, pp. 884–886, Aug. 2011.

[15] N. Sambo *et al.*, "Routing code and spectrum assignment (RCSA) in elastic optical networks," *J. Lightw. Technol.*, vol. 33, no. 24, pp. 5114–5121, Dec. 2015.

[16] M. Salani, C. Rottondi, and M. Tornatore, "Routing and spectrum assignment integrating machine-learning-based QoT estimation in elastic optical networks," in *Proc. IEEE INFOCOM - IEEE Conf. Comput. Commun.*, Apr. 2019, pp. 1738–1746.

[17] F. Zhang, Q. Zhuge, and D. V. Plant, "Fast analytical evaluation of fiber nonlinear noise variance in mesh optical networks," *IEEE/OSA J. Opt. Commun. Netw.*, vol. 9, no. 4, pp. C88–C97, Apr. 2017.

[18] D. J. Ives, P. Bayvel, and S. J. Savory, "Physical layer transmitter and routing optimization to maximize the traffic throughput of a nonlinear optical mesh network," in *Proc. Int. Conf. Opt. Netw. Design Model.*, May 2014, pp. 168–173.

[19] S. J. Savory, "Congestion aware routing in nonlinear elastic optical networks," *IEEE Photon. Technol. Lett.*, vol. 26, no. 10, pp. 1057–1060, May 2014.

[20] D. J. Ives, P. Bayvel, and S. J. Savory, "Routing, modulation, spectrum and launch power assignment to maximize the traffic throughput of a nonlinear optical mesh network," *J. Lightw. Technol.*, vol. 29, no. 3, pp. 244–256, 2015.

[21] R. J. Vincent, D. J. Ives, and S. J. Savory, "Scalable capacity estimation for nonlinear elastic all-optical core networks," *J. Lightw. Technol.*, vol. 37, no. 21, pp. 5380–5391, Nov. 2019.

[22] M. Cantono *et al.*, "On the interplay of nonlinear interference generation with stimulated Raman scattering for QoT estimation," *IEEE / OSA J. Lightw. Technol.*, vol. 36, no. 15, pp. 3131–3141, Aug. 2018.

[23] I. Roberts, J. M. Kahn, J. Harley, and D. W. Boertjes, "Channel power optimization of WDM systems following Gaussian noise nonlinearity model in presence of stimulated raman scattering," *J. Lightw. Technol.*, vol. 35, no. 23, pp. 5237–5249, 2017.

[24] A. Mitra, D. Semrau, N. Gahlawat, A. Srivastava, P. Bayvel, and A. Lord, "Effect of reduced link margins on C+L band elastic optical networks," *IEEE/OSA J. Opt. Commun. Netw.*, vol. 11, no. 10, pp. C86–C93, Oct. 2019.

[25] A. Mitra, D. Semrau, N. Gahlawat, A. Srivastava, P. Bayvel, and A. Lord, "Effect of channel launch power on fill margin in c+l band elastic optical networks," *J. Lightw. Technol.*, vol. 38, no. 5, pp. 1032–1040, Mar. 2020.

[26] J. Bromage, "Raman amplification for fiber communications systems," *J. Lightw. Technol.*, vol. 22, no. 1, pp. 79–93, Jan. 2004.

[27] M. Cantono, A. Ferrari, D. Pilori, E. Virgillito, J. Augé, and V. Curri, "Physical layer performance of multi-band optical line systems using raman amplification," *J. Optical Commun. Netw.*, vol. 11, no. 1, pp. A103–A110, 2019.

[28] A. Ferrari, A. Tanzi, S. Piciaccia, G. Galimberti, and V. Curri, "Selection of amplifier upgrades addressed by quality of transmission and routing space," in *Proc. Opt. Fiber Commun. Conf. Exhib.*, 2019, pp. 1–3.

[29] S. Aozasa *et al.*, "Tm-doped fiber amplifiers for 1470-nm-band WDM signals," *Photon. Technol. Lett.*, vol. 12, no. 10, pp. 1331–1333, Oct. 2000.

[30] Fiberlabs-Inc, "Praseodymium fluoride fiber glass doped amplifier," Dec. 9, 2018. [Online]. Available: www.fiberlabs.com

[31] E. Dianov, "Bismuth-doped optical fibers: A challenging active medium for near-IR lasers and optical amplifiers," *Light: Sci. Appl.*, vol. 1, p. e12, 2012.

[32] M. Filer and S. Tibuleac, "N-degree ROADM architecture comparison: Broadcast-and-select versus route-and-select in 120 Gb/s DP-QPSK transmission systems," in *Proc. Opt. Fiber Commun. Conf.*, Mar. 2014, pp. 1–3.

[33] M. Filer, M. Cantono, A. Ferrari, G. Grammel, G. Galimberti, V. Curri, "Multi-vendor experimental validation of an open source qot estimator for optical networks," *J. Lightw. Technol.*, vol. 36, no. 15, pp. 3073–3082, 2018.

[34] V. Curri, M. Cantono, R. Gaudino, "Elastic all-optical networks: A new paradigm enabled by the physical layer. How to optimize network performances?" *J. Lightw. Technol.*, vol. 35, no. 6, pp. 1211–1221, 2017.

[35] A. Ferrari *et al.*, "GNPy: An open source application for physical layer aware open optical networks," *IEEE/OSA J. Opt. Commun. Netw.*, vol. 11, no. 10, pp. C94–C108, Jun. 1, 2020.

[36] A. Ferrari *et al.*, "Experimental validation of an open source quality of transmission estimator for open optical networks," in *Proc. Opt. Fiber Commun. Conf.*, Mar. 2020, pp. 1–3.

[37] D. Semrau, R. I. Killey, and P. Bayvel, "The gaussian noise model in the presence of inter-channel stimulated raman scattering," *J. Lightw. Technol.*, vol. 36, no. 14, pp. 3046–3055, Jul. 2018.

[38] I. Roberts, J. M. Kahn, J. Harley, and D. W. Boertjes, "Channel power optimization of WDM systems following Gaussian noise nonlinearity model in presence of stimulated Raman scattering," *J. Lightw. Technol.*, vol. 35, no. 23, pp. 5237–5249, 2017.

[39] D. Semrau, R. I. Killey, and P. Bayvel, "A closed-form approximation of the Gaussian noise model in the presence of inter-channel stimulated raman scattering," *J. Lightw. Technol.*, vol. 37, no. 9, pp. 1924–1936, 2019.

[40] E. W. Dijkstra, "A note on two problems in connexion with graphs," *Numerische Mathematik*, vol. 1, pp. 269–271, 1959.

[41] N. Sambo, F. Cugini, G. Bottari, P. Iovanna, and P. Castoldi, "Distributed setup in optical networks with flexible grid," in *Proc. 37th Eur. Conf. Exhib. Opt. Commun.*, Sep. 2011, pp. 1–3.

[42] V. Curri *et al.*, "Design strategies and merit of system parameters for uniform uncompensated links supporting Nyquist-WDM transmission," *J. Lightw. Technol.*, vol. 33, no. 18, pp. 3921–3932, 2015.